Research Paper

Antiviral/antibacterial biodegradable cellulose nonwovens as environmentally friendly and bioprotective materials with potential to minimize microplastic pollution

Chao Deng [a], Farzad Seidi [a,*], Qiang Yong [a,*], Xiangyu Jin [d], Chengcheng Li [a], Xing Zhang [a], Jingquan Han [a], Yuqian Liu [a], Yang Huang [a], Yuyan Wang [c], Zhenghong Yuan [c], Huining Xiao [b,*]

[a] *International Innovation Center for Forest Chemicals and Materials and Jiangsu Co-Innovation Center for Efficient Processing and Utilization of Forest Resources, Nanjing Forestry University, Nanjing 210037, China*
[b] *Department of Chemical Engineering, University of New Brunswick, Fredericton, NB, Canada E3B 5A3*
[c] *Key Laboratory of Medical Molecular Virology (MOE/NHC/CAMS), Department of Medical Microbiology and Parasitology, School of Basic Medical Sciences, Shanghai Medical College, Fudan University, Shanghai 200032, China*
[d] *Engineering Research Center of Technical Textiles, Ministry of Education, College of Textiles, Donghua University, Shanghai 201620, China*

ARTICLE INFO

ABSTRACT

Personal protective equipment (PPE) such as face masks is vital in battling the COVID-19 crisis, but the dominant polypropylene-based PPE are lack of antiviral/antibacterial activities and environmental friendliness, and have hazardous impact on the soil and aquatic ecosystems. The work presented herein focused on developing biodegradable, antiviral, and antibacterial cellulose nonwovens (AVAB-CNWs) as a multi-functional bioprotective layer for better protection against coronavirus SARS-CoV-2 and addressing environmental concerns raised by the piling of COVID-19 related wastes. Both guanidine-based polymer and neomycin sulfate (NEO) were reactive-modified and covalently grafted onto the surface of cellulose nonwovens, thereby conferring outstanding antiviral and antibacterial activities to the nonwovens without deteriorating the microstructure and biodegradability. Through adjusting the grafting amount of active components and selecting appropriate reagents for pretreatment, the antimicrobial activity and hydrophobicity for self-cleaning of the nonwovens can be tuned. More importantly, we demonstrated for the first time that such multi-functional nonwovens are capable of inactivating SARS-CoV-2 instantly, leading to high virucidal activity (> 99.35%), which is unachievable by conventional masks used nowadays. Meanwhile, the robust breathability and biodegradability of AVAB-CNWs were well maintained. The applications of the as-prepared nonwovens as high-performance textile can be readily extended to other areas in the fight against COVID-19.

1. Introduction

The use of personal protective equipment (PPE), such as N95 filtering facepiece respirators (FFR) and surgical masks, remains an important mitigation strategy against the severe acute respiratory syndrome coronavirus 2 (SARS-CoV-2) until people are actually vaccinated or even afterwards due to the emergence of new COVID-19 variant (Leung et al., 2020; Ortega et al., 2020; Ranney et al., 2020). However, lack of antiviral and antibacterial properties allows the long-time survival of bacteria or viruses on the surface of PPE including face masks (Chin and Poon, 2020; Sachan, 2020), which can readily induce cross-contamination and post-infection, thus resulting in their short service life and an immense amount of disposal. On the other hand, the dominant material of PPE available in the market is polypropylene (PP)-based, which, however, is non-biodegradable and partially responsible for the current burden of plastic pollution with 250,000 tons per day (Dean, 2020; Klemeš et al., 2020; Kumar et al., 2020a, 2020b; Parashar and Hait, 2021; Patricio Silva et al., 2021), and has created ecotoxicological effects on soil ecosystems where the PP fragments are bio-fragmentated into microplastics by uptake, ingestion, and egestion of soil species, thus leading to those nano- and microplastics distributed and dispersed in soil ecosystems (Huerta Lwanga et al., 2018; Kwak and An, 2021a, 2021b). Moreover, the PP-based face mask is once discarded in the aquatic environment, millions of microplastic fibers can be

released in water, causing the enormous concerns in marine ecosystems (Morgana et al., 2021). On account of environmental sustainability and economic benefits, developing biodegradable face masks coped with antimicrobial and antiviral activities without compromising the filtration performance and breathability is of extreme importance.

Various techniques have been attempted to improve the self-sterilization and antimicrobial properties of the nonwoven fabrics of face masks (Seidi et al., 2021), such as coating with salt (Quan et al., 2017; Rubino et al., 2020), metal nanoparticles (Kumar et al., 2020a, 2020b; Zhong et al., 2020a, 2020b, 2020c), and the incorporation of graphene (Chua et al., 2020; Huang et al., 2020; Shan et al., 2020; Zhong et al., 2020a, 2020b, 2020c) and photosensitizers in the mask layers (Horvath et al., 2020; Monge et al., 2020; Tang et al., 2020). Despite noteworthy progress in last year in the construction of functional nonwoven fabrics of face masks, enormous challenges still remain for practical applications of these functional-modified face masks: (i) most of the modifications have been performed on non-biodegradable PP-based nonwoven fabric which has already created significant environmental concerns after disposal (Chen et al., 2021; Kwak and An, 2021a, 2021b; Morgana et al., 2021); (ii) most of these functional nonwoven fabrics require an external stimulus (including light, voltage, and pressure) to trigger the functions which practically limits the applications. For instance, those requiring light will not be useful in dark conditions (Horvath et al., 2020; Tang et al., 2020); whereas the functional agents requiring voltage to activate often rely on a battery carried by users (Kim et al., 2021; Shan et al., 2020); (iii) poor adhesion between the water-soluble modifying agents (such as inorganic salts, essential oils, and quaternary ammonium compounds) with the nonwoven fabrics is another issue. Thus, fixation of such modifiers to the nonwoven layers for the elimination of leaching-out of active components is essential to reduce the toxicity and maintain the long-term effectiveness of the nonwoven fabrics. Hence, the biodegradable fabrics with the functions similar to PP or better are particularly appealing.

In fact, the green-based and biodegradable materials for antimicrobial/antiviral face masks tend to be elusive. To date, the most developed biodegradable and antimicrobial materials are the electrospun nanofiber mats that use gluten (Das et al., 2020), PLA/chitosan (Wibisono et al., 2020), licorice extract (Chowdhury et al., 2021), and silk fibroin (Belda Marin et al., 2020) as raw materials. However, the use of these nanofiber layers decreases the airflow, making the face mask less breathable to some extent. To tackle the issues associated with environmental concerns while enhancing the protective and breathing performance of face masks, developing bio-based or compostable nonwoven fabrics endowed with bactericidal and virucidal activity is extremely important in the current or even future pandemic. To meet such demands, two challenges must be addressed: 1) exploring the disinfectants with high antiviral and antibacterial activity, which can also be covalently grafted on nonwoven fabrics for sustainable and long-term effectiveness; 2) identifying proper green-based nonwoven fabrics with desirable porous structures for proper breathing. Among various relevant antimicrobial polymers, the guanidine-based polymer has been well received due to its strong antibacterial and antiviral properties with high biocompatibility, making it a promising agent applied in various fields such as medicine, packaging, food, and agriculture (Li et al., 2016; Li et al., 2018; Pan et al., 2019; Zhang and Xiao, 2013). The guanidine-based polymers can inactivate the bacteria and viruses effectively through damaging the cell membrane or capsids of bacteria and viruses and interaction with the thiol groups of cellular proteins, thus leading to the leakage of cytoplasmic components (Qin et al., 2020; Sun et al., 2010; Zhong et al., 2020a, 2020b, 2020c). The polymers can also be covalently grafted on various substrates, including the star polymers consisting of guanidine-based arms developed in our previous work, which were found effective not only against bacterium (E. coli) but also non-enveloped adenovirus (ADV) (Pan et al., 2015). However, whether guanidine-based polymer remains its effectiveness in inactivating enveloped virus, SARS-CoV-2 in particular, is still unknown. This

has literally stimulated our research on exploring such a polymer for rendering biodegradable nonwoven fabrics antiviral. It is worth noting that our previous work has clearly demonstrated that the incorporation of guanidine antimicrobial polymer into biodegradable resins (e.g., PBAT/starch blends) has minimal detrimental effect on the biodegradability of substrates due to limited dosage used (Wang et al., 2015; Wei et al., 2016). On the other hand, neomycin sulfate (NEO), a kind of water-soluble aminoglycoside antibiotic, exhibits efficient antibacterial performance against both Gram-positive and Gram-negative bacterial strains (Ilkar Erdagi et al., 2020; Jabeen et al., 2017), and has also been reported to possess antiviral property (Alazard-Dany et al., 2019; Zhang et al., 2009). It can be transported into the cytoplasm of bacteria to interfere with the protein synthesis (Becker and Cooper, 2013; Malvika Kaul, 2004). This has led to another alternative to incorporate the antibiotics that have been proved to be capable of endowing the biodegradable nonwoven fabrics with antiviral/antibacterial activities.

Based on those aforementioned, an ideal PPE must have inherent and stable long-term self-sterilization and does not raise the environmental burdens after disposal. Here, we designed antiviral and antibacterial cellulosic fiber-based nonwovens (AVAB-CNWs) as biodegradable and breathable protective layer, in an attempt to meet the unprecedented demand on developing personal protective equipment (PPE) with enhanced performance and the least environmental impact in the current COVID-19 pandemic or even afterwards. The biodegradable nonwovens consist of the regenerated cellulose fibers originating from the most abundant natural resources in the world (Gross and Kalra, 2002; Li et al., 2021). By successfully grafting of the polyhexamethylene guanidine (PHMG) or NEO on the surface of the CNWs which exhibit significant antibacterial activity against both E. coli and S. aureus, thus effectively preventing bacterial infections of PPE. More importantly, the highly effective antiviral property against SARS-CoV-2 allows AVAB-CNWs to act as a superior alternative layer for substituting the conventional and non-biodegradable layers in PPE. In addition, the hydrophobic-modified AVAB-CNWs facilitate the rolling, sliding, and repelling of water droplets, contributing to the self-cleaning and antifouling properties of PPE. Meanwhile, with the appropriate air permeability, the comfortable breathability of AVAB-CNWs is maintained when they are applied in face masks. Considering the integration of biodegradability, breathability, antiviral and antibacterial activities, the findings from this work enable us to create the safe, comfortable, and environmental-friendly cellulose nonwovens with the applications expandable from masks, leading to emerging and high-performance materials for PPE in the fight against COVID-19 pandemic.

2. Materials and methods

2.1. Materials

Pristine cellulose nonwovens (CNWs) fabricated from pulp and lyocell fibers were provided by Zhejiang Hezhong Nonwoven Company and used as the starting material of the antiviral and antibacterial cellulose nonwovens (AVAB-CNWs). N, N-Dimethylformamide (DMF, 99.5%), cyclohexyl isocyanate (98%), dibutyltin dilaurate (DBTL, 95%), triethylamine (99%), thiourea (99%), methacryloyl chloride (95%), ethylene carbonate (98%), 4-hydroxybenzophenone (98%), glycidyl methacrylate (GMA, 97%) and neomycin sulfate (NEO, USP grade) were purchased from Aladdin Biochemical Technology Co., LTD. Dioxane (99%) was purchased form Macklin Biochemical Technology Co., LTD. Polyhexamethyleneguanidine (PHMG) was self-synthesized according to the procedures reported by Guan et al. in our previous work (Guan et al., 2007). Sodium hydrogen carbonate and ethanol were purchased from Lingfeng Chemical Reagent Co. LTD. and Yasheng Chemical Co., LTD, respectively.

2.2. AVAB-CNWs preparation

CNWs were cut into a rectangular shape of size 14 × 16 cm, then dried in a vacuum oven at 90 °C for 5 h before grafting with cyclohexyl isocyanate as a coupling agent. The dried CNWs were added in the reacting solvent consisting of 50 mL of DMF, 10 mL of cyclohexyl isocyanate (CI) and 125 μL of dibutyltin dilaurate. The entire reaction system was then kept at 100 °C for 1 h. The as-prepared CNWs-CI were washed with ethanol for three times and dried at ambient temperature. Afterwards, the PTB solution with a concentration of 7 mg mL^{-1} was prepared by dissolving 420 mg PTB in 60 mL dioxane. Then, CNWs-CI and CNWs were dipped into the PTB solvent for 5 min respectively and took out to dry at ambient temperature. After drying, the as-prepared CNWs-CI-PTB and CNWs-PTB were treated by UV irradiation (365 nm) for 5 min with each side. Subsequently, the PHMG and NEO solutions were prepared by dissolving 12 g PHMG and NEO in 60 mL deionized (DI) water respectively, and the pH of both solutions were kept high than 7. Finally, the CNWs-CI-PTB and CNWs-PTB were both immersed in PHMG and NEO solutions at 80 °C for 24 h. The as-obtained AVAB-CNWs (CNWs-CI-PTB-PHMG/NEO and CNWs-PTB-PHMG/NEO) were washed with DI water for one time and then ethanol for three times, and dried at ambient temperature.

2.3. Measurements and characterization

The morphology of CNWs at different grafting steps was observed using a field emission scanning electron microscope (FE-SEM). The FE-SEM experiment was conducted with a Hitachi JSM-7600F SEM working at an acceleration voltage (5 kV). Water contact angles of samples were examined using a T200-Auto 3 Plus contact angle analyzer (BiolinScientific, Germany). A drop of distilled water with amount of 4 μL from a micro syringe was automatically dispensed on the surface of sample. Fourier-transform infrared (FTIR) analyses of the samples were performed on a VERTEX80v spectrometer (Bruker Optik GmbH, Germany) with the scanning range of 400–4000 cm^{-1} (2 cm^{-1} resolution). Raman spectra were obtained using a DXR532 laser Raman spectrometer (Thermo Fisher Scientific, USA) to determine the changing of functional groups in the chemical reactions. X-ray photoelectron spectrometer (XPS) measurements were carried out using an AXIS UltraDLD spectrometer (Kratos, UK) to determine the chemical states of the samples at different grafting steps. The chemical composition and structures of synthesized reagents and related materials were determined using AVANCE III HD 600 MHz NMR spectrometer (Bruker Biospin, Switzerland) and 400 MHz solid NMR spectrometer (Bruker Biospin, Switzerland), respectively. The element content data of samples were collected by the elemental analyzer (2400 II, Perkin Elmer, USA). Mechanical tests were performed on an Autograph AGS-X tensile tester (SHIMADZU, Japan) with the stretching rate of 50 mm min^{-1}. The samples were cut into size of 50 mm in length and 6 mm in width. Air permeability evaluations were conducted using a digital air permeability tester (YG461E, Wenzhou Fangyuan Instrument Co., Ltd, China), in which the sample size is 250 × 250 mm^2.

2.4. Antibacterial assay using E. coli and S. aureus

For antibacterial activity experiments, the colony count method was utilized to quantitatively evaluate the inhibition efficiency of cell growth. In the colony count method, both gram-negative *E. coli* and gram-positive *S. aureus* were used to investigate the antibacterial properties of the AVAB-CNWs. In particular, the bacterial strains of *E. coli* and *S. aureus* were incubated overnight in Luria-Bertani (LB) broth medium with shaking at 200 rpm at 37 °C. The bacterial suspension was then diluted with LB broth to a concentration of 5 × 10^6 colony-forming units CFU/mL. After that, 0.1 g AVAB-CNWs sample was mixed with 5 mL diluted bacterial suspension in the vial, and subsequently shook at 200 rpm at 37 °C. At 10 min and 60 min, 100 μL of suspensions were taken out and coated on gelatinous LB agar plates respectively, culturing at 37 °C for 24 h. The number of colonies was counted and the growth inhibition rate (GIR) was estimated by the formula: GIR = (A − B)/A × 100%, in which the A and B are the number of the bacterial colonies counted from the control and AVAB-CNWs samples, respectively. The experiments were repeated three times for each bacteria.

2.5. Antiviral assay using HCoV-229E virus

For HCoV-229E antiviral activity tests, the Madin-Darby Canine Kidney (MDCK) was used to breed the HCoV-229E virus at 34 °C. The AVAB-CNWs and control samples were cut into a size of 20 × 20 mm^2, and 0.2 mL of virus suspension was spotted on the surface of samples in the vials which were then incubated at 25 °C for 60 min. After incubation, 20 mL of Soybean Casein Digest Lecithin Polysorbate (SCDLP) medium were added, and the virus was eluted by vortex for 5 s and 5 times. Subsequently, virus suspension was immediately diluted serially, and 0.1 mL of the dilution was used to infect MDCK cells seeded previously at a density of 10^4 cells per well, followed by incubation for 1 h at 34 °C with 5% CO$_2$. Afterwards, the maintenance medium (0.2 mL) was added in the well incubated at 34 °C with 5% CO$_2$. After 7 days, the cytopathy of the cell was monitored using inverted microscopy, and TCID$_{50}$ was calculated.

2.6. Antiviral assay using SARS-CoV-2 virus

For SARS-CoV-2 antiviral assay, the SARS-CoV-2 SH01 strain (GenBank accession no. MT121215) isolated from a COVID-19 patient by passaging in Vero E6 cells was used. VeroE6 cells were seeded a day prior to the assay in 96-well plates. Five drops of 20 μL (100 μL total) of virus suspension were spotted on the surface of AVAB-CNWs samples in a size of 2 × 2 cm^2 and exposed for 0.1, 10, 30 min at 25 °C. At each time point, the samples with the virus were added 10 mL of EBSS, and were then vortexed for 5 s and stirred for 5 times. Subsequently, 0.1 mL of virus solution was mixed with 0.9 mL of maintenance medium, and serially diluted. 0.1 mL of virus dilutions were plated in each well and incubated for 1 h at 37 °C with 5% CO$_2$. Afterwards, 100 μL of methyl cellulose were added in each well, and incubated at 37 °C with 5% CO$_2$. After 48 h incubation, the plates were added 4% paraformaldehyde (200 μL per well) for 30 min, then transferred to 0.2% saponin solution for stanning. Cells were stained with rabbit against SARS-CoV N protein polyclonal antibody overnight at 4 °C, then incubated with the secondary goat anti-rabbit HRP-conjugated antibody for 2 h at room temperature. The focus-forming unit was developed using TrueBlue substrate (Sera Care #5510-0030). Plaques were counted using the inverted microscopy, and reported as PFU mL^{-1}, where PFU refers to a plaque-forming unit. All data were standardized as 1 × 10^5 PFU initial load and plotted PFU.

2.7. Cell viability assays

The MTT assay was used to evaluate the cytotoxicity of AVAB-CNWs samples. In a typical experiment, NIH3T3 cells were cultured in cell growth media (87% DMEM, 10% FBS, 1% sodium pyruvate, 1% glutamine, and 1% nonessential amino acids). Samples were required to have UV-sterilization at least 30 min for both sides before put in a 48-well plate, and 100 μL of growth medium was used as control. Afterwards, the AVAB-CNWs samples were seeded by NIH3T3 cells with an initial density of 1 × 10^4 cells per well and incubated for 24 h (37 °C, 5% CO$_2$). After that, AVAB-CNWs samples and growth medium were removed, and PBS was used to wash the wells for three times. Subsequently, growth medium containing MTT (0.5 mg mL^{-1}) was added in each well (200 μL) and then incubated for 4 h (37 °C, 5% CO$_2$). The plate was then gently shaken for 10 min after adding 200 μL of DMSO to sufficiently mix the solution. The cell viability was determined by observing the absorbance change at 570 nm using an UV–visible spectrometer.

2.8. Filtration performance

For filtration performance tests, the AVAB-CNWs samples were stacked on meltblown nonwovens (20 g m^{-2}) that were procured from Xuancheng Guangneng Nonwovens CO., Ltd., then measured by an Automated Filter Tester 8130 (TSI, USA) using a flow rate of 85 L min^{-1} and sodium chloride (NaCl) as the aerosol with a mass median diameter of 0.26 μm. Each sample was measured at least three times and average results were reported.

3. Results and discussion

3.1. Fabrication and characteristics of AVAB-CNWs

A facile strategy for the fabrication of antiviral and antibacterial cellulose nonwovens (AVAB-CNWs) is shown in detail in Fig. 1. The synthesis of CNWs-CI-PTB-PHMG/NEO involves three steps: 1) controlled hydrophobization of the surface of nonwoven by reacting cellulosic hydroxyls with cyclohexyl isocyanate (CI); 2) UV-induced grafting of the poly(thiiran-2-yl methyl methacrylate-2-(4-benzoyl phenoxy)ethyl methacrylate) (PTB) on the surface of the as-obtained CNWs-CI and 3) grafting of antiviral/antibacterial agents by the ring-opening reaction of the thiirane with primary amino groups of PHMG or NEO. In parallel, direct UV-grafting of the PTB on the surface of pristine nonwovens was also performed, followed by coupling with PHMG or NEO. In fact, the surface of unmodified nonwovens is highly hydrophilic due to the inherent characteristics of cellulose, whereas the pre-functionalization with CI renders the surface of CNWs extremely hydrophobic. Hence, the biodegradable CNWs-CI-PTB-PHMG/NEO is designed to replace the conventional spunbond nonwovens as the outer layer of PPE with self-cleaning and virucidal/biocidal functions, reducing the risk of infection and prolonging the usage of PPE materials. As for CNWs-PTB-PHMG/NEO without CI pre-treatment, it is targeted as the middle layer combined with meltblown nonwovens to endow PPE with antiviral and antibacterial properties. Such unique design and

fabrication strategies, via both hydrophobic and hydrophilic routes, allow the modified CNWs applicable to different kinds of PPE materials according to their own characteristics and application environments.

To manifest the successful covalent conjugation over each grafting step, X-ray photoelectron spectroscopy (XPS) was used to identify the elemental composition on the material surface. XPS wide scan spectra of AVAB-CNWs are depicted in Fig. 2a, b. Apparently, the N 1s peak appeared in the CNWs-CI (Fig. 2a), implying the presence of C—N bond (Fig. 2e) when compared with the C 1s core-level spectra of CNWs (Fig. 2i). The S 2p peak exhibited in the CNWs-CI-PTB (Fig. 2a) and CNWs-PTB (Fig. 2b), suggesting the presence of C-S or thiirane group (Fig. 2f, j). Note that a new peak at 288.4 eV (C=N) in the XPS spectra of CNWs-CI-PTB-PHMG (Fig. 2g) indicated the successful attachment of PHMG to CNWs-CI-PTB, compared with the C 1s core-level spectra of CNWs-CI-PTB (Fig. 2f). Peaks with binding energies of 163.4, 164.5 and 167.9 eV appeared in the S 2p core-level spectra of CNWs-CI-PTB-NEO (Fig. 2h) indicated the presence of S$_{2p3/2}$ C—S—C, S$_{2p1/2}$ C—S—C and SH—C bonds, thus confirming the grafting of NEO onto the surface of CNWs-CI-PTB. Compared with CNWs-PTB (Fig. 2j), new peaks at 285.0 eV (C-N) and 288.4 eV (C=N) in the C 1s core-level spectra of CNW-PTB-PHMG verified the successful connection of PHMG to CNW-PTB (Fig. 2k). Similarly, the successful linkage of NEO onto the CNWs-PTB was confirmed by the new peak at C-N (285.0 eV) (Fig. 2l). Overall, the results from XPS clearly demonstrated the success in the preparation of AVAB-CNWs.

The grafting of different chemicals on CNWs via covalent bonding was also confirmed from the FTIR spectra presented in Fig. 2c, d. Comparing the spectrum of CNWs-CI with that of CNWs, new absorption peaks at 1715 and 1525 cm^{-1} were observed in the spectrum of CNWs-CI, which were assigned to the carbonyl group and N-H bending of the carbamate linkage, thus confirming the successful conjugation of CI onto CNWs (Fig. 2c). Moreover, the introduction of cyclohexyl groups increased the intensity of the peaks related to C-H groups at 2928 cm^{-1} and 2854 cm^{-1}. The grafting of PTB is evidenced by the presence of benzene ring at 705 cm^{-1}. After the PHMG grafting, the characteristic
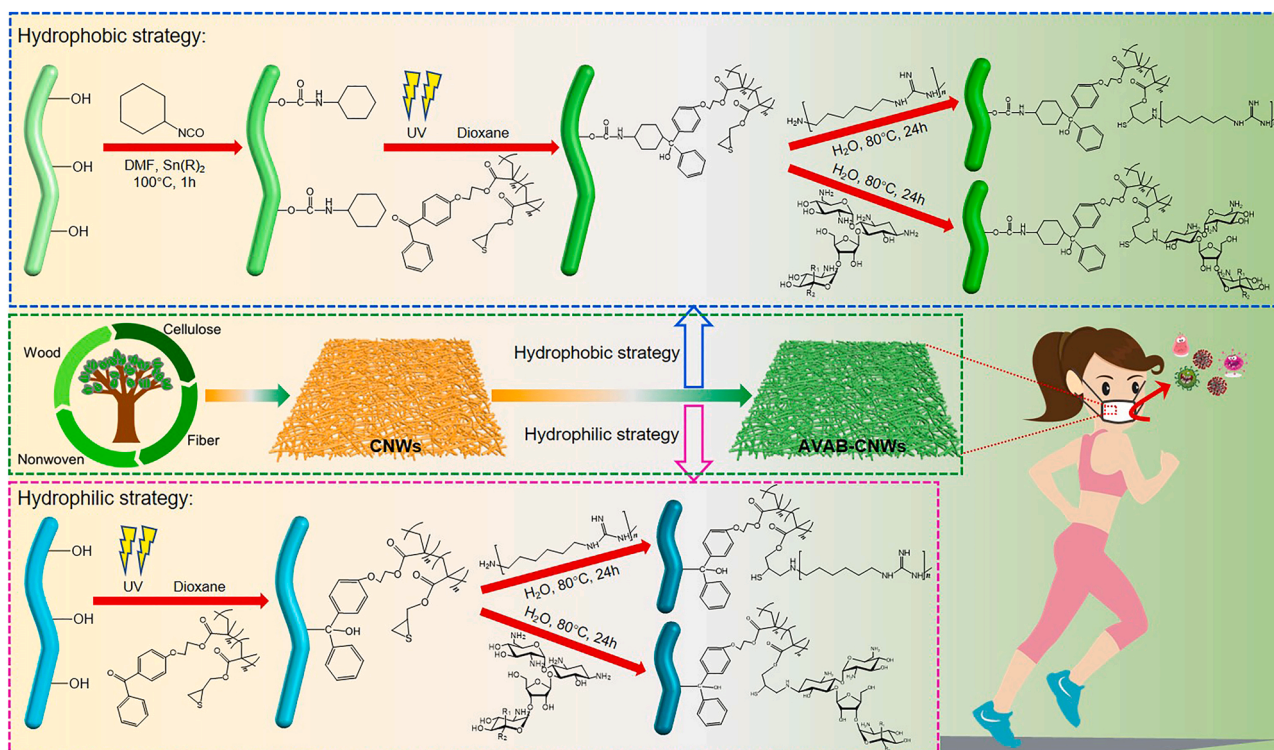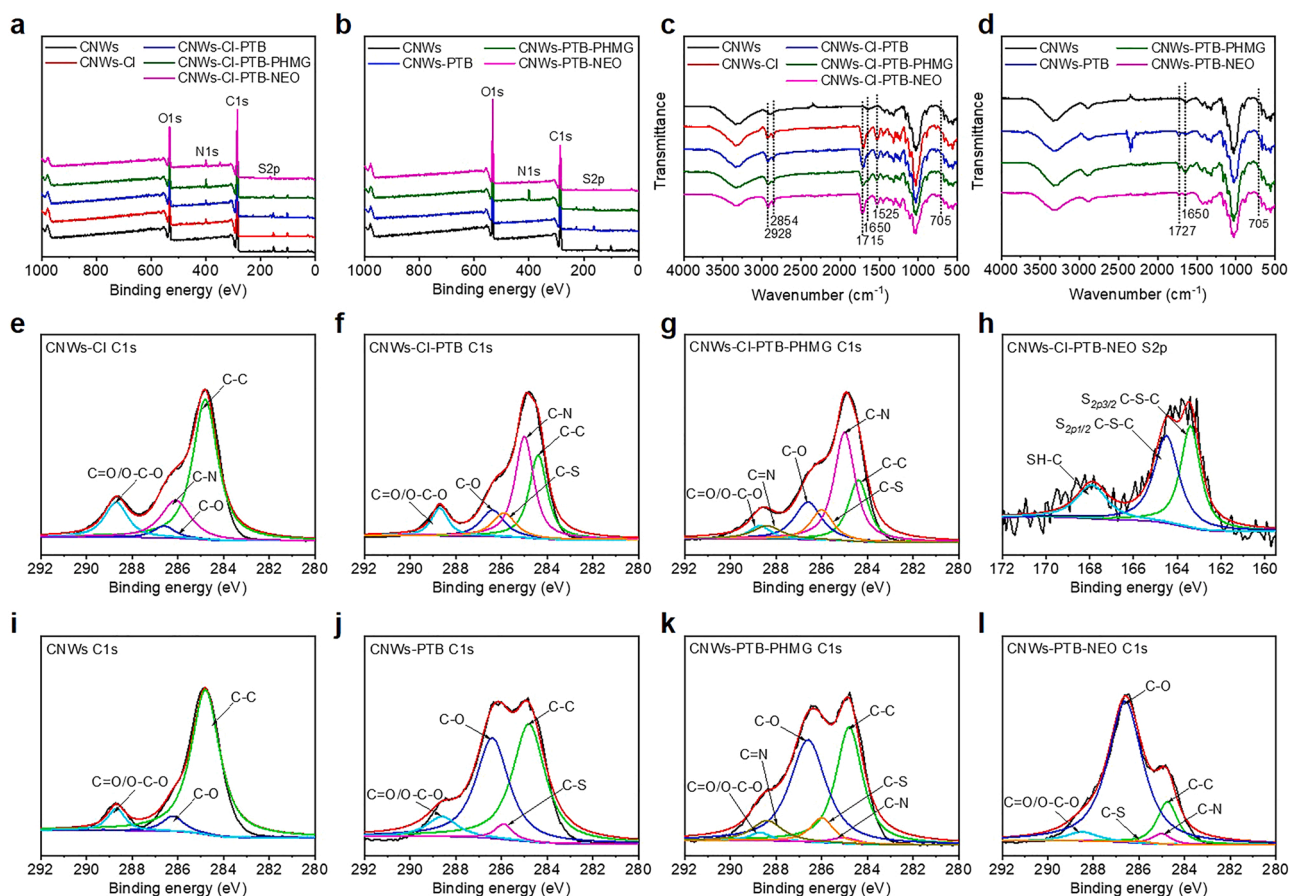

Fig. 1. Overall design and fabrication of antiviral and antibacterial cellulose nonwovens (AVAB-CNWs) based on biodegradable and regenerated cellulose nonwovens via two robust methodologies: hydrophobic (upper) and hydrophilic (lower) strategies.

Fig. 2. Demonstration of polymer grafting on CNWs. (a, b) Wide scan XPS spectra. (c, d) FTIR spectra. (e–g) C 1s core-level spectra of CNWs-CI, CNWs-CI-PTB and CNWs-CI-PTB-PHMG. (h) S 2p core-level spectra of CNWs-CI-PTB-NEO. (i–l) C 1s core-level spectra of CNWs, CNWs-PTB, CNWs-PTB-PHMG and CNWs-PTB-NEO.

absorption peak at 1650 cm^{-1} in the curve of CNWs-CI-PTB-PHMG spectrum, assigned to C=N stretching vibration, suggested the existence of PHMG in the sample.

The successful preparation of CNWs-PTB was confirmed by the characteristic bands of the ester bond at 1727 cm^{-1}, and the C=C of benzene ring at 705 cm^{-1} (Fig. 2d) after PTB grafting. The peak at 1650 cm^{-1} in the CNWs-PTB-PHMG spectrum represents the guanidine groups in PHMG, confirming that the PHMG was successfully grafted on the surface of CNWs-PTB. Meanwhile, FTIR provided little information on the grafting of NEO due to the overlap of signals related to NEO with those of the functional groups in CNW. However, the presence of NEO was confirmed from other results including XPS, CHNS, and water contact angle.

Additionally, the Raman spectra of pristine and modified CNWs are presented in Fig. S1a, b. Raman and FTIR are two non-destructive techniques for monitoring the changes in the functional groups of materials during a sequential modification. Indeed, the frequency positions of the groups identified by FTIR and Raman are usually identical but generally with reverse intensities. The new Raman signal at 800 cm^{-1} in the spectrum of CNWs-CI is related to the CH$_2$ groups originating from the inserted cyclohexane moieties. Additionally, the intensity of the signal at around 2900–2950 cm^{-1} was increased significantly due to the inserted CH$_2$ groups. After coating the CNWs-CI or CNWs with PTB, new signals appeared at 615 and 1720 cm^{-1} which are attributed to the C-S from thiirane group and carbonyl of the ester group of the grafted PTB layer. Furthermore, in the Raman spectra of CNWs-CI-PTB-PHMG, CNWs-CI-PTB-NEO, CNWs-PTB-PHMG, and CNWs-PTB-NEO, the intensity of the signal at 615 cm^{-1} was reduced due to the opening of the thiirane ring upon reaction with the amino groups in NEO or PHMG.

Further confirmation for the successful modification of CNWs was

obtained by comparing the solid ^{13}C NMR of pristine CNWs with CNWs-CI-PTB-PHMG as an example of modified nonwovens. As depicted in Fig. S2, the ^{13}C NMR spectrum of CNWs clearly showed the characteristic peaks of cellulose in the range of 50–110 ppm. Meanwhile, several new signals appeared in the ^{13}C NMR spectrum of CNWs-CI-PTB-PHMG (Fig. S3), including those related to the carbonyl (C=O) moieties of esters and urethane groups in the range of 170–180 ppm, as well as the C=N guanidine unit around 155 ppm. The signal of the four CH$_2$ groups of inserted cyclohexane, CH$_3$ groups of the PTB chains, and three CH$_2$ groups of PHMG all appeared together in the range of 16–37 ppm; whereas the signals of the CH$_2$ groups of PTB backbone and carbons neighbor to the electronegative groups including the CH$_2$-N and CH$_2$-O can be found in the range of 40–60 ppm. Due to the low content (5 mol %) of the aromatic groups in the PTB structure, very weak signals for the aromatic groups appeared in the range of 110–125 ppm.

To quantitatively determine the final amounts of PHMG and NEO grafted onto CNWs, the elemental analysis was carried out; and the results are listed in Table S1. The data from the elemental analysis of CNWs and CNWs-CI showed a higher content of nitrogen for CNWs-CI, which could prove the introduction of the urethane bond. The slight decrease of N% of CNWs-CI-PTB is reasonable due to the grafting of PTB which has no nitrogen. However, the higher contents of nitrogen in CNWs-CI-PTB-PHMG and CNWs-CI-PTB-NEO, compared to that in CNWs-CI-PTB, demonstrated the successful grafting of PHMG and NEO. According to the results, the quantitative contents of PHMG and NEO moieties incorporated in AVAB-CNWs (C_{PHMG} and C_{NEO} (mg g^{-1})) were 34.37 and 27.03 mg g^{-1}, respectively. However, for the CNWs-PTB-PHMG and CNWs-PTB-NEO samples, C_{PHMG} and C_{NEO} were lower than those of the samples pretreated by CI. This can be explained by the increased reactive sites from CI by introducing more CH$_2$ groups to the

material surface, which in turn induce the more efficient radical coupling reaction with PTB, thus leading to higher C_{PHMG} and C_{NEO} for CNWs-CI-PTB-PHMG and CNWs-CI-PTB-NEO.

Typical morphology of the CNWs is shown in SEM images (Fig. 3a). The surface of CNWs has small pores with diameter of ~ 100 µm (Fig. S4) which contributes to appropriate air permeability of CNWs. Microscopically, the overall morphological and porous structure of nonwoven remains almost intact after functionalization with CI (Fig. 3b). In contrast, the morphology of CNWs-CI-PTB (Fig. 3c) clearly shows a very thin and dense layer of PTB uniformly coated on the surface of fibers, interconnecting the fibers via the thin film formed. By omitting the pre-functionalization step with CI, CNWs were directly immersed into the PTB solution; and the microstructure of as-obtained CNWs-PTB appears to be similar to that before modification (see Fig. 3f), though the surface of fibers is less covered by the polymer, as depicted by the magnified SEM images. This most likely resulted from the lack of CI grafting step, which reduced the amount of PTB grafted on the surface. The microstructures of as-fabricated CNWs-CI-PTB-PHMG/ NEO are shown in Fig. 3d, e. As can be seen, the thin layer remained on the surface of fibers after the grafting of PHMG or NEO. However, the nonwovens presented relatively more porous and fluffy structure compared to CNWs-CI-PTB (Fig. S5). From the SEM images in Fig. 3g, h, it is clear that the as-prepared CNWs-PTB-PHMG/NEO still possessed

fluffy three-dimensional structures compared to those of CNWs-CI-PTB-PHMG/NEO which are slightly different due to the introduction of hydrophobic groups by CI in the materials. Moreover, as flexible as traditional nonwovens used in filter media, AVAB-CNWs can be readily rolled-up, folded, and recovered (see Fig. 3i) and are highly feasible for application in PPE-related materials.

The hydrophilicity and hydrophobicity of the modified CNWs prepared over different routes were also characterized in terms of the water contact angles (WCA). It has been well accepted that the cellulosic fibers are highly hydrophilic, which was also confirmed by the rapid reduction of WCA of pristine CNWs from initial 74.1° to 0° after 2 s (Fig. 3j(i)). Such a high absorption rate towards water is ascribed to the bulky three-dimensional structure and porous structure of CNWs (see Fig. 3a). However, the immobilization of cyclohexyl groups strongly enhanced the hydrophobicity of CNWs-CI, leading to WCA up to 128.0° which remained unchanged even after 180 s (Fig. 3j(ii)). Grafting of PTB showed negligible effect on the hydrophobicity (Fig. 3j(iii)) due to the similar hydrophobicity raised by PTB. However, grafting of PHMG and NEO agents lowered WCA values marginally to 117.7° and 118.6°, respectively, for CNWs-CI-PTB-PHMG and CNWs-CI-PTB-NEO (Fig. 3j (iv), j(v)). The slight reduction of hydrophobicity is due to the hydrophilic nature of PHMG and NEO, thus further demonstrating the presence of such antimicrobial chains or groups on the surface of CNNWs.
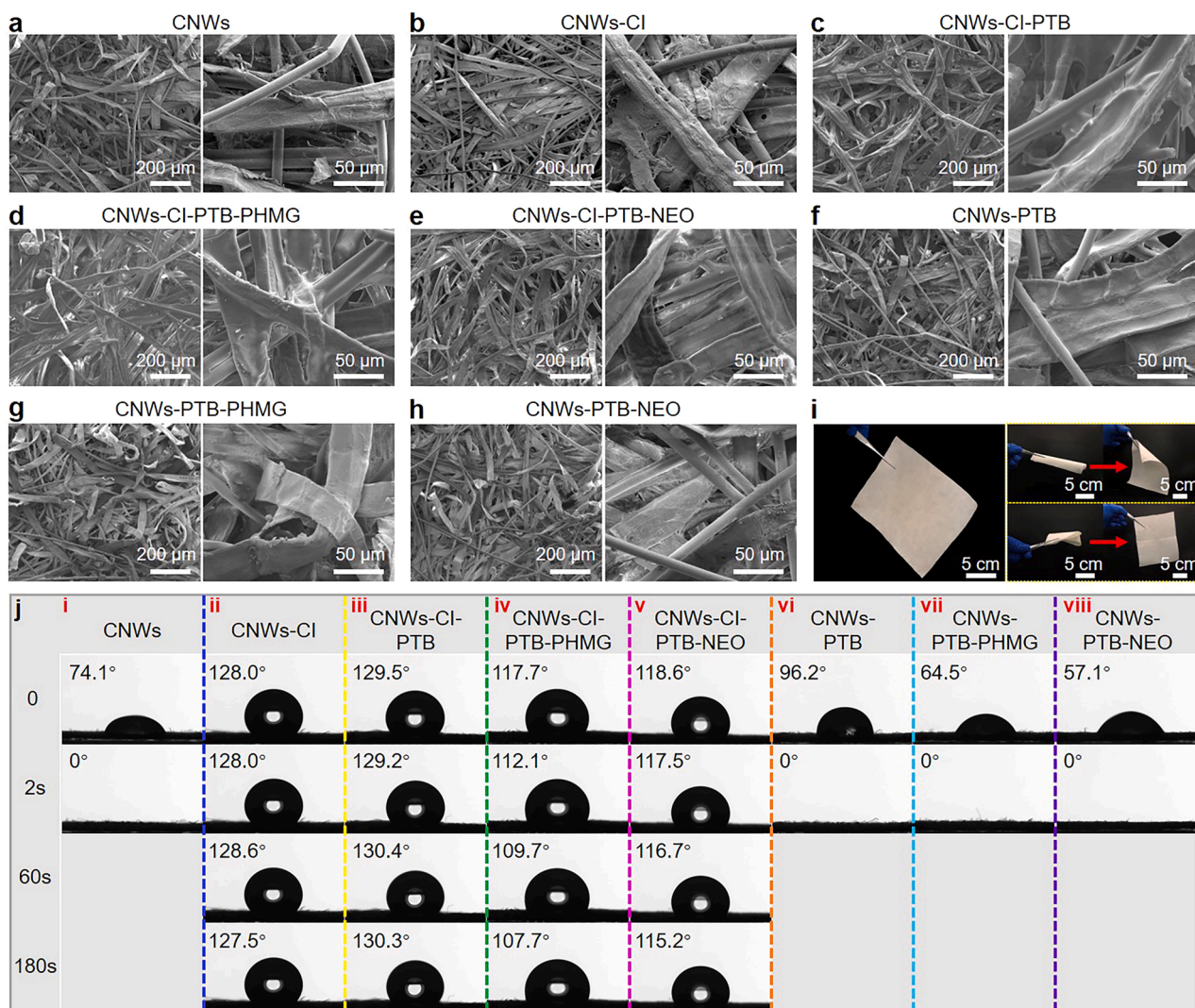

Fig. 3. Fabrication and characterization of AVAB-CNWs. (a–h) SEM images of the microscopic structures of CNWs at every grafting step. (i) Optical images of AVAB-CNWs that can be rolled up, folded, and recovered. (j) Photographs of the water contact angle of CNWs at every grafting step.

Since the water absorption rate can be indirectly represented by the reduction of WCA as a function of time (Fu et al., 2020), it can be seen from Fig. 3j(iv), j(v) that the reduction is higher for CNWs-CI-PTB-PHMG (10.0° over 180 s) than that of CNWs-CI-PTB-NEO (3.4° over 180 s), which may be attributed to the higher amount of PHMG grafted (3.44%) in comparison to the NEO (2.70%). Moreover, despite the increased hydrophobicity of the nonwoven grafted with PTB, the water absorption rate was as high as the pristine CNWs. This most likely resulted from the well-maintained fluffy structure so that water droplet could be easily absorbed. After grafting of hydrophilic PHMG and NEO, the initial contact angles of CNWs-PTB-PHMG and CNWs-PTB-NEO were reasonably decreased, while retaining high water absorption rates (Fig. 3j(vii), j(viii)). The versatile AVAB-CNWs endowed with different hydrophilicity and hydrophobicity by different synthesis methods enable them applicable to various PPE materials, such as the covering layer (CNWs-CI-PTB-PHMG/NEO) in medical face mask media and inner shaping layer (CNWs-PTB-PHMG/NEO) combined with PP meltblown nonwovens in N95 respirator media.

3.2. Antibacterial/antiviral activities of AVAB-CNWs

On account of the significance of bio-protection of PPE, their antibacterial/antiviral activity is of extreme importance. PHMG and NEO are recognized as excellent antimicrobial agents with broad-spectrum biocidal properties for various applications (Pan et al., 2016; Zhong et al., 2021). Here, a colony counting method was used to quantify the antibacterial activities of the AVAB-CNWs against two representing pathogenic bacteria, i.e., Gram-negative E. coli and Gram-positive

S. aureus (Cui et al., 2021). The photographs of bacterial colonies after 10 min and 60 min exposure to the samples are shown in Fig. 4a, and the corresponding growth inhibition rates are presented in Fig. 4b–e. On the plate of the control sample after 10 min contact, the remarkable bacterial growth occurred regardless of the type of bacteria. The relatively robust bacterial growth, especially the S. aureus, also appeared for CNWs-CI-PTB-PHMG. Whereas almost no survival bacterial colonies were observed for the plates of CNWs-PTB-PHMG after 10 min contact, indicating stronger inhibitory effects of the CNWs-PTB-PHMG on both bacterial strains compared with those of the CNWs-CI-PTB-PHMG. This could be related to the potential reduction of bacterial adhesion caused by the hydrophobic surface of CNWs-CI-PTB-PHMG, leading to less probability of bacterial inactivation upon contact. The growth inhibition rates of CNWs-CI-PTB-PHMG and CNWs-PTB-PHMG against E. coli and S. aureus were about 83.37% ± 3.42%, 72.74% ± 3.91% and > 99.99%, 99.99% ± 0.01%, respectively (Fig. 4b, c). However, when the contact time was prolonged to 60 min, both CNWs-CI-PTB-PHMG and CNWs-PTB-PHMG samples exhibited excellent bactericidal efficacy (nearly >99.99%) for both E. coli and S. aureus (Fig. 4b, c). The results imply that the contact time plays an important role for CNWs-CI-PTB-PHMG and CNWs-PTB-PHMG to inactivate bacteria.

The antibacterial activities of the CNWs-CI-PTB-NEO and CNWs-PTB-NEO with comparison of the control sample after 10 min and 60 min are also displayed in Fig. 4a. As can be seen, both CNWs-CI-PTB-NEO and CNWs-PTB-NEO only exhibited limited inactivating capability against the E. coli after 10 min contact, with growth inhibition rates of 45.74% ± 3.42% and 71.45% ± 3.92%, respectively (Fig. 4d); whereas the antibacterial activity against S. aureus was much higher with the
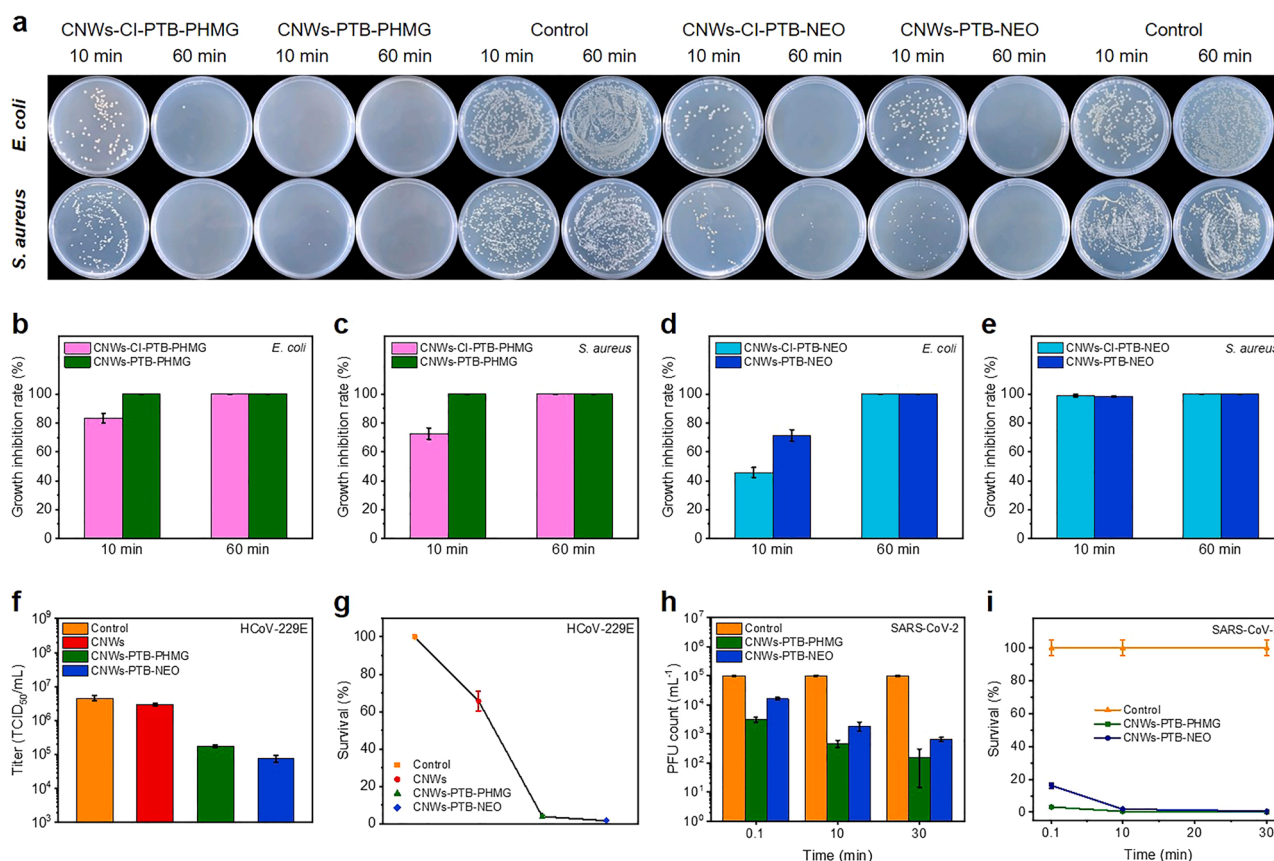
Fig. 4. Antibacterial/antiviral activities of AVAB-CNWs. (a) Optical images of colonies of E. coli and S. aureus of AVAB-CNWs and control samples after 10 min and 60 min contact time (10^5 CFU/mL). (b–e) Growth inhibition rate (GIR) of AVAB-CNWs against E. coli and S. aureus after 10 min and 60 min contact time. (f) Infectivity of the HCoV-229E virus on different AVAB-CNWs at exposure time of 60 min (g) Survival of the HCoV-229E virus on different AVAB-CNWs. (h) Biocidal assay against SARS-CoV-2 virus for different AVAB-CNWs at different exposure time. (i) Survival of the SARS-CoV-2 virus on different AVAB-CNWs at different exposure time.

inactivating rates up to 99.06% ± 0.87% and 98.43% ± 0.39%, respectively (Fig. 4e). Hence, it is speculated that NEO polymer has better inactivating capability against *S. aureus* compared to *E. coli* within short time. This might be caused by different structures of bacteria with different cell membrane constituents, where *S. aureus* has an outer peptidoglycan layer while *E. coli* has an outer phospholipid membrane (Ilkar Erdagi et al., 2020). As for the contact time at 60 min, both CNWs-CI-PTB-NEO and CNWs-PTB-NEO exhibited significantly anti-bacterial functions due to their decomposition effects on the cell membrane of bacteria (Fig. 4a), resulting in the growth inhibition rates of against *E. coli* and *S. aureus* were as high as > 99.99%, 99.99% ± 0.01% and > 99.99%, > 99.99%, respectively (Fig. 4d, e). When the enzymes are inactivated, the cell wall attached with NEO is subsequently destroyed, allowing NEO to penetrate inside the cell to bound to the DNA and deactivate the organisms (Asabuwa Ngwabebhoh et al., 2018; Ilkar Erdagi et al., 2020). Moreover, the as-prepared AVAB-CNWs have no leaching effect according to the results of inhibition zone assays (Figs. S6–S9), indicating their potential applications in PPE without worrying about the safe concerns. Based on the experimental results, it can be concluded that grafting PHMG or NEO endowed AVAB-CNWs with outstanding antibacterial activities, leading to promising applications in protective medical materials.

To validate the antiviral function of AVAB-CNWs which is more important in the current work, the antiviral performance against HCoV-229E (Human coronavirus) and SARS-CoV-2 viruses (Covid-19 related) were tested; and the cytopathic effect was evaluated using a Titer assay. HCoV-229E is a type of coronavirus with less virulent capacity, and thus was selected as a surrogate on several AVAB-CNWs samples prior to the SARS-CoV-2 inactivation tests. As shown in Fig. 4f, nearly no contact inactivation was observed on the pristine CNWs, and the titer of CNWs ($10^{6.47}$ TCID$_{50}$/mL) was marginally decreased compared to that of control virus suspension ($10^{6.66}$ TCID$_{50}$/mL) (Table S2). In contrast, both CNWs-PTB-PHMG and CNWs-PTB-NEO showed effective inactivation of HCoV-229E virus, achieving titers of $10^{5.25}$ and $10^{4.89}$ TCID$_{50}$/mL, respectively after 60 min contact exposure. To express the antiviral performance more intuitively, HCoV-229E Survival, which is defined as the ratio of a titer at a given exposure time normalized relative to that of the control virus suspension multiplied by 100%, was calculated (Fig. 4g). The results showed that the survival rates of HCoV-229E were 65.71% ± 5.28%, 3.93% ± 0.69% and 1.73% ± 0.41% for the pristine CNWs, CNWs-PTB-PHMG and CNWs-PTB-NEO, respectively. Compared with CNWs-PTB-PHMG, CNWs-PTB-NEO seems to have better inactivating effect on HCoV-229E. The positive results based on HCoV-229E demonstrate for the first time that the cellulose-based nonwoven grafted with the reactive chains containing guanidine and NEO segments is highly effective against coronavirus. More importantly, the virucidal activities of AVAB-CNWs verified from HCoV-229E testing literally encouraged us to proceed with identifying their activity against SARS-CoV-2, which is critical for the application of the antiviral PPE-related materials in the current pandemic or even afterwards.

As can be seen from Fig. 4h, both CNWs-PTB-PHMG and CNWs-PTB-NEO showed rapid and effective inactivation of SARS-CoV-2, achieving 2.8 and 2.2 log of PFU (plaque-forming units) reduction within 30 min of contact, respectively. Noteworthily, the PFU reductions of these two AVAB-CNWs can reach 1.5 and 0.8 log, respectively, after momentary contact (~ 0.1 min), highlighting the fast and high virucidal activities (Table S3). Such positive results demonstrated the effectiveness of both CNWs-PTB-PHMG and CNWs-PTB-NEO nonwoven in rapidly inactivating SARS-CoV-2 for the first time. The survival of SARS-CoV-2 on the AVAB-CNWs is presented as a function of exposure time in Fig. 4i. Comparing to the control SARS-CoV-2 virus suspension, the survival of SARS-CoV-2 after instant contact (~ 0.1 min) with CNWs-PTB-PHMG and CNWs-PTB-NEO were 3.17% ± 0.61% and 16.23% ± 1.69%, respectively, confirming the instant inactivating abilities, especially for the PHMG modified CNWs. After 30 min contact exposure, the inactivation rates of CNWs-PTB-PHMG and CNWs-PTB-NEO reached

99.84% ± 0.14% and 99.35% ± 0.11%, respectively, validating that the AVAB-CNWs inactivates SARS-CoV-2 over the course of minutes. Moreover, compared with the results associated with HCoV-229E, the SARS-CoV-2 has shown more susceptibility to the AVAB-CNWs further confirming the suitability and effectiveness of the AVAB-CNWs used as PPE to prevent the viral transmission in the current and post-pandemic.

The antiviral mechanism of AVAB-CNWs relies on the guanidine-segments and NEO grafted on the surface of cellulose nonwoven along with the hydrophobic modification of the substrates. The viral inactivation probably consists of two steps: (i) adsorption or trapping of the virus on the surface of the modified layer, (ii) inactivation of the virus by grafted PHMG or NEO. The antiviral protection of PHMG may result from the interaction of PHMG polycations with the plasma membrane of target cell that protects the enveloped virus, and the strong binding of polycations with membrane phospholipids that screen the cell from virus (Lysytsya and Mandygra, 2014). In other words, PHMG segments on the surface of AVAB-CNWs may induce the disorganization and severe damage of lipid envelope of coronavirus due to the interaction between the polycations and viral particles, leading to the leakage of the viral genome. In addition, low pH in the endosome is required for the replication of virus infections (Ichiyama et al., 2016). The unprotonated amine groups in guanidine-based polymers might neutralize the endosomal pH, thus preventing viral infection due to low pH-induced virus-cell membrane fusion. As for NEO, the possibility is that NEO may directly inhibit SARS-CoV-2 through specifically interacting with the viral structural or binding to viral RNA (Zhang et al., 2009). The amine groups in NEO might also neutralize the endosomal pH and play the role similar to those in PHMG. Moreover, the antiviral result of NEO is in agreement with reports that aminoglycosides inhibit replication of DNA and RNA viruses in several species (Bottero et al., 2013). Therefore, both guanidine-based polymer and NEO, once covalently grafted on cellulose surface after reactive modification, render cellulose nonwoven highly antiviral from a mechanistic point of view, thus enabling the nonwovens especially suitable as performance-enhance bio-protective materials which are unachievable by conventional materials used in PPE.

3.3. Cytotoxicity, mechanical properties, filtration performance, and breathability of AVAB-CNWs

Considering the bio-protection applications, cytotoxicity is an important parameter to assess the material safety. As shown in Fig. 5a, the NIH3T3 cell viability values of CNWs-CI-PTB-PHMG, CNWs-CI-PTB-NEO, CNWs-PTB-PHMG, and CNWs-PTB-NEO were 56.33% ± 7.15%, 75.29% ± 14.67%, 43.45% ± 5.23%, and 86.57% ± 12.29%, respectively. The results suggested the higher biocompatibility of NEO than PHMG agent which is also consistent with the findings from the fluorescent images of live/dead assays (Figs. 5b–d and S10a, b). Although PHMG grafted AVAB-CNWs showed relatively low cell viability values, it is still higher than that of the AgNPs modified biocidal masks (~ 30%) even treated with extremely low concentration of AgNPs (5 μg mL^{-1}) (Szczepańska et al., 2020). Furthermore, since the AVAB-CNWs are used as the outer layer of the mask and do not contact the human skin directly, thus guaranteeing the biosafety of the face masks when AVAB-CNWs are incorporated.

Practically, the introduced AVAB-CNWs are supposed to replace the polypropylene spunbond nonwovens (PP SBNWs) layer in commercial masks. Accordingly, mechanical properties were measured and compared to evaluate the durability of the masks against mechanical forces. As depicted in Fig. 5e, the AVAB-CNWs showed higher tensile strength with lower ductility compared to those of PP SBNWs, indicating good practical performance when incorporated in face masks as outer layer. Moreover, the calculated elastic modulus of AVAB-CNWs (exclude CNWs-CI-PTB-PHMG) was higher than that of PP SBNWs (Fig. S11), reaching as much as nearly 4 times (292.8 MPa vs 75.7 MPa), which proved the excellent resistance to external physical damage in daily
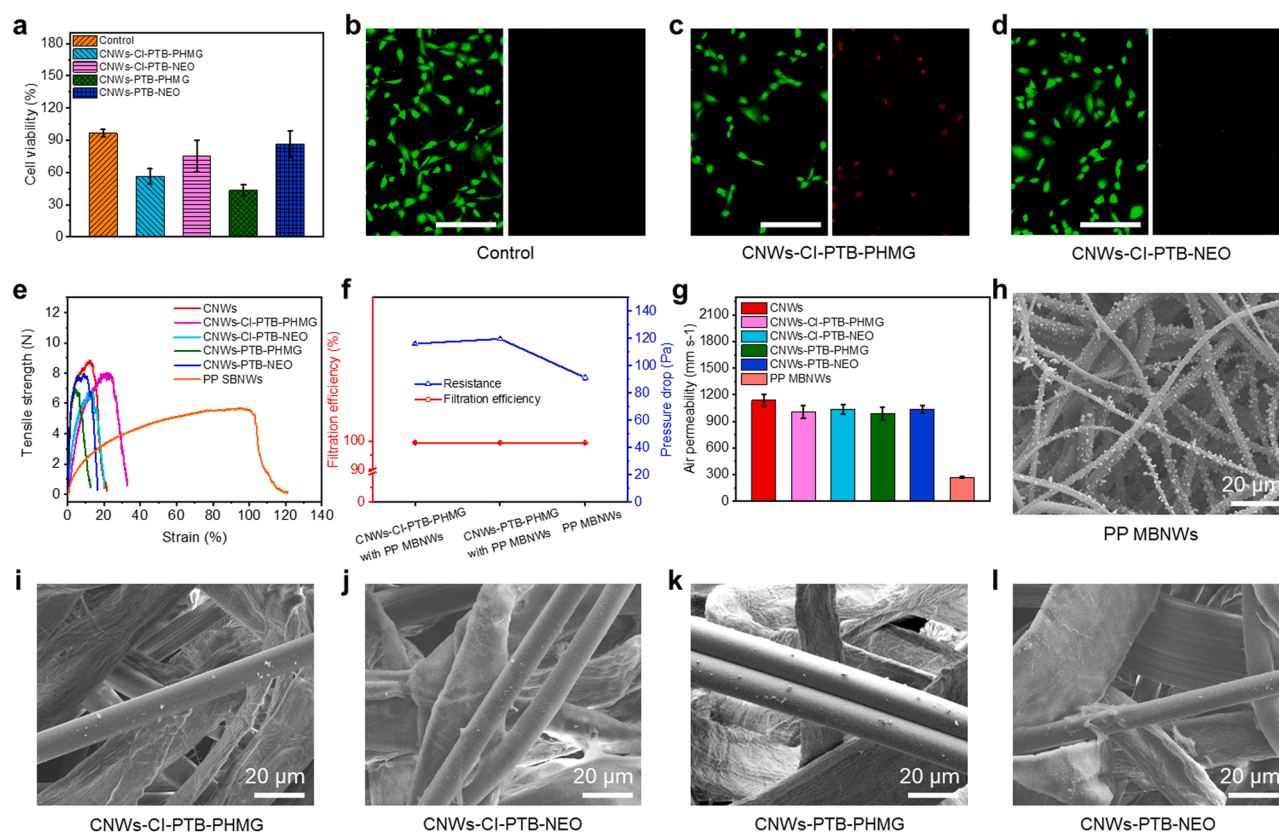
Fig. 5. Cytotoxicity, mechanical properties, breathability, and filtration performance of AVAB-CNWs. (a) The cell viability. (b–d) Live/dead images of control, CNWs-Cl-PTB-PHMG, and CNWs-Cl-PTB-NEO (scale bar: 20 μm). (e) Tensile strength of different AVAB-CNWs compared with commercial PP spunbond nonwovens. (f) Filtration efficiency, pressure drop, and (g) air permeability of AVAB-CNWs combined with PP MBNWs vs single PP MBNWs. (h–l) SEM images of sodium chloride particles capture of PP MBNWs and AVAB-CNWs after the loading filtration test.

usage.

The interception property is one of the important features of PPE. Hence, it is worth exploring whether the AVAB-CNWs layer has impact on the filtration properties of the entire filtering media. We combined the AVAB-CNWs layer with polypropylene meltblown nonwovens (PP MBNWs) typically used in face masks to examine the filtration property which was compared with that of a single PP MBNWs. As depicted in Figs. 5f, S12, all four AVAB-CNWs samples combined with PP MBNWs possessed the high filtration efficiency (> 99%) comparable with the PP MBNWs, suggesting that the face masks can maintain excellent filtration performance when the functional AVAB-CNWs are used as alternatives for other layers in face masks. Meanwhile, the filtration efficiencies of AVAB-CNWs and PP SBNWs were also investigated (Fig. S13). The obtained results showed that the AVAB-CNWs had more than 1.63-fold higher filtration efficiency (7.5% vs 4.6%) than the commercial PP SBNWs, which further demonstrated the superiority of the AVAB-CNWs as outer layer of face masks. The pressure drops of the AVAB-CNWs combined with PP MBNWs were relatively higher (up to 119 Pa) compared to that of PP MBNWs (94 Pa), which might be attributed to the increased numbers of fibers of combined layers leading to the increased thickness and tortuous airflow channels that cause the increase of pressure drop. However, the performance still meet the requirement of the standard about "Technical specification of day protective mask" (Zhang et al., 2019).

In addition, the air permeabilities of AVAB-CNWs and PP MBNWs were detected to further evaluate the breathability of AVAB-CNWs. Compared to the air permeability of PP MBNWs (271.6 ± 7.2 mm s^{-1}), all the AVAB-CNWs possess much higher air permeability in the range of ~ 900–1000 mm s^{-1}, which is about 3 times as high as PP MBNWs (Fig. 5g). The results further demonstrated

that the green-based AVAB-CNWs not only create excellent barrier against a broad spectrum of bacteria and viruses (coronavirus in particular), but also possess prominent breathability, thus guaranteeing the superior performance of the PPE integrated with AVAB-CNWs as a biodegradable substitute layer for hot-air nonwovens or PP spunbond nonwovens in filtering media. Moreover, the morphologies of AVAB-CNWs and PP MBNWs after filtration loading for 20 min were visualized with SEM (Fig. 5h–l), in which sodium chloride particles were used as model particles for aerosols and microorganisms. Clearly, the deposition of sodium chloride particles on the surface of the PP fibers are visible due to the electrostatic attraction, inertial impaction, mechanical interception, and diffusion by Brownian motion which is the predominant filtration mechanism when the aerosol size is in the 100 nm to 1 μm range (Konda et al., 2020; Tcharkhtchi et al., 2021) (Fig. 5h), whereas the AVAB-CNWs can also capture some small particles on their surface (Fig. 5i–l). This unique behavior implies that the AVAB-CNWs can improve the aerosol filtering performance of face masks.

Overall, the multi-functional AVAB-CNWs are promising as scalable virucidal materials and feasible as biodegradable layers in PPE-related materials. It is worth noting that the low dosage of antiviral/antibacterial components used in the current systems will not deteriorate the biodegradability of cellulose nonwoven though might slightly prolong the period for complete degradation (Wei et al., 2016). Therefore, replacing the non-biodegradable PP-based face masks used dominantly nowadays with AVAB-CNWs will not only minimize the environmental impact after disposal, but also endow the face masks with superior performance unachievable by traditional petroleum-based nonwovens. Multi-layered masks could be fabricated by combining AVAV-CNWs with different types of cellulose-based nonwoven or cotton, resulting in completely biodegradable face masks with high performance.

Moreover, the strategies we developed in the current work for rendering CNWs antiviral/antibacterial and self-cleaning are applicable to all kind of cellulose-based materials such as packaging materials, hospital-used textiles, and high-efficiency particulate air (HEPA) filters for aircrafts etc. Therefore, the application of the as-prepared biodegradable and multi-functional nonwoven as advanced materials can be extended to a variety of areas, thus magnifying their benefits substantially.

4. Conclusions

In summary, we have successfully grafted highly effective antiviral/ antibacterial components on surfaces of cellulose nonwoven fabric via unique covalent linkages and created a breathable, multi-functional and biodegradable nonwoven layer for PPE-related materials. The as-prepared AVAB-CNWs possess adjustable hydrophobicity and the controllable amount of antiviral/antibacterial segments on the surface of cellulosic nonwovens, and provide an ideal outer layer of PPE for effectively repelling the aqueous droplets or aerogels bearing contagious bacteria and viruses. The intrinsic structures of antiviral/antibacterial agent resulted in the decomposition of bacterial cell membrane, endowing the nonwoven with excellent growth inhibition towards both *E. coli* and *S. aureus*. Most importantly, for the first time we demonstrated that the cellulose nonwovens grafted with reactive-modified PHMG and NEO could create a range of fascinating AVAB-CNWs which showed the extremely high and instant antiviral activities against coronavirus, SARS-CoV-2 in particular. Such unique performance is mainly attributed to the effective destruction of protein synthesis induced by virucidal components incorporated on the surfaces of the nonwoven. Moreover, by using such cellulose nonwoven layer as an alternative for petro-derived nonwoven layers in surgical or non-surgical masks and N95 respirator, we anticipate that the rising environment pollution caused by COVID-19-related wastes can be eased due to the biodegradable and self-cleaning characteristics of these disposable face masks. Notably, we anticipate that replacing the PP-based masks by the cellulose ones significantly reduce the amount of micro-/ nano-plastics which are considered as new sources of soil and water pollutants. In conjunction with other nonwoven materials, especially cellulose-based biodegradable ones as other layers, the AVAB-CNWs created in this work could generate a variety of antiviral textiles as high-performance materials. The application of such specialty textile is not limited to the face masks in the fight against COVID-19, and can be extended to various types of PPE and the high-efficiency particulate air filters for aircrafts and vehicles etc.

CRediT authorship contribution statement

Chao Deng: Conceptualization, Methodology, Validation, Formal analysis, Investigation, Data curation, Writing – original draft, Writing – review & editing. **Farzad Seidi:** Supervision, Methodology, Validation, Writing – review & editing. **Qiang Yong:** Investigation, Resources, Funding acquisition. **Xiangyu Jin:** Investigation, Resources, Methodology. **Chengcheng Li:** Methodology, Validation. **Xing Zhang:** Formal analysis, Software. **Jingquan Han:** Validation, Formal analysis. **Yuqian Liu:** Formal analysis, Software. **Huang Yang:** Formal analysis. **Yuyan Wang:** Methodology, Validation. **Zhenghong Yuan:** Methodology, Validation. **Huining Xiao:** Conceptualization, Supervision, Project administration, Writing – review & editing, Funding acquisition.

Declaration of Competing Interest

The authors declare that they have no known competing financial interests or personal relationships that could have appeared to influence the work reported in this paper.

Acknowledgements

Appendix A. Supplementary material

Supplementary data associated with this article can be found in the online version at doi:10.1016/j.jhazmat.2021.127391.

References

Alazard-Dany, N., Denolly, S., Boson, B., Cosset, F.L., 2019. Overview of HCV life cycle with a special focus on current and possible future antiviral targets. Viruses 11, 30.

Asabuwa Ngwabebhoh, F., Ilkar Erdagi, S., Yildiz, U., 2018. Pickering emulsions stabilized nanocellulosic-based nanoparticles for coumarin and curcumin nanoencapsulations: in vitro release, anticancer and antimicrobial activities. Carbohydr. Polym. 201, 317–328.

Becker, B., Cooper, M.A., 2013. Aminoglycoside antibiotics in the 21st century. ACS Chem. Biol. 8, 105–115.

Belda Marin, C., Fitzpatrick, V., Kaplan, D.L., Landoulsi, J., Guenin, E., Egles, C., 2020. Silk polymers and nanoparticles: a powerful combination for the design of versatile biomaterials. Front. Chem. 8, 604398.

Bottero, V., Sadagopan, S., Johnson, K.E., Dutta, S., Veettil, M.V., Chandran, B., 2013. Kaposi's sarcoma-associated herpesvirus-positive primary effusion lymphoma tumor formation in NOD/SCID mice is inhibited by neomycin and neamine blocking angiogenin's nuclear translocation. J. Virol. 87, 11806–11820.

Chen, X., Chen, X., Liu, Q., Zhao, Q., Xiong, X., Wu, C., 2021. Used disposable face masks are significant sources of microplastics to environment. Environ. Pollut. 285, 117485.

Chin, A.W.H., Poon, L.L.M., 2020. Stability of SARS-CoV-2 in different environmental conditions – authors' reply. Lancet Microbe 1, 146.

Chowdhury, M.A., Shuvho, M.B.A., Shahid, M.A., Haque, A., Kashem, M.A., Lam, S.S., Ong, H.C., Uddin, M.A., Mofijur, M., 2021. Prospect of biobased antiviral face mask to limit the coronavirus outbreak. Environ. Res. 192, 110294.

Chua, M.H., Cheng, W., Goh, S.S., Kong, J., Li, B., Lim, J.Y.C., Mao, L., Wang, S., Xue, K., Yang, L., Ye, E., Zhang, K., Cheong, W.C.D., Tan, B.H., Li, Z., Tan, B.H., Loh, X.J., 2020. Face masks in the new COVID-19 normal: materials, testing, and perspectives. Research 2020, 7286735.

Cui, F., Sun, J., Ji, J., Yang, X., Wei, K., Xu, H., Gu, Q., Zhang, Y., Sun, X., 2021. Carbon dots-releasing hydrogels with antibacterial activity, high biocompatibility, and fluorescence performance as candidate materials for wound healing. J. Hazard. Mater. 406, 124330.

Das, O., Neisiany, R.E., Capezza, A.J., Hedenqvist, M.S., Forsth, M., Xu, Q., Jiang, L., Ji, D., Ramakrishna, S., 2020. The need for fully bio-based facemasks to counter coronavirus outbreaks: a perspective. Sci. Total Environ. 736, 139611.

Dean, R., 2020. PPE: polluting planet earth. Br. Dent. J. 229, 267.

Fu, Q., Tu, K., Goldhahn, C., Keplinger, T., Adobes-Vidal, M., Sorieul, M., Burgert, I., 2020. Luminescent and hydrophobic wood films as optical lighting materials. ACS Nano 14, 13775–13783.

Gross, R.A., Kalra, B., 2002. Biodegradable polymers for the environment. Science 297, 803–807.

Guan, Y., Xiao, H., Sullivan, H., Zheng, A., 2007. Antimicrobial-modified sulfite pulps prepared by in situ copolymerization. Carbohydr. Polym. 69, 688–696.

Horvath, E., Rossi, L., Mercier, C., Lehmann, C., Sienkiewicz, A., Forro, L., 2020. Photocatalytic nanowires-based air filter: towards reusable protective masks. Adv. Funct. Mater. 30, 2004615.

Huang, L., Xu, S., Wang, Z., Xue, K., Su, J., Song, Y., Chen, S., Zhu, C., Tang, B.Z., Ye, R., 2020. Self-reporting and photothermally enhanced rapid bacterial killing on a laser-induced graphene mask. ACS Nano 14, 12045–12053.

Huerta Lwanga, E., Thapa, B., Yang, X., Gertsen, H., Salanki, T., Geissen, V., Garbeva, P., 2018. Decay of low-density polyethylene by bacteria extracted from earthworm's guts: a potential for soil restoration. Sci. Total Environ. 624, 753–757.

Ichiyama, K., Yang, C., Chandrasekaran, L., Liu, S., Rong, L., Zhao, Y., Gao, S., Lee, A., Ohba, K., Suzuki, Y., Yoshinaka, Y., Shimotohno, K., Miyakawa, K., Ryo, A., Hedrick, J., Yamamoto, N., Yang, Y.Y., 2016. Cooperative orthogonal macromolecular assemblies with broad spectrum antiviral activity, high selectivity, and resistance mitigation. Macromolecules 49, 2618–2629.

Ilkar Erdagi, S., Asabuwa Ngwabebhoh, F., Yildiz, U., 2020. Genipin crosslinked gelatin-diosgenin-nanocellulose hydrogels for potential wound dressing and healing applications. Int. J. Biol. Macromol. 149, 651–663.

Jabeen, S., Islam, A., Ghaffar, A., Gull, N., Hameed, A., Bashir, A., Jamil, T., Hussain, T., 2017. Development of a novel pH sensitive silane crosslinked injectable hydrogel for controlled release of neomycin sulfate. Int. J. Biol. Macromol. 97, 218–227.

Kim, Y.I., Kim, M.W., An, S., Yarin, A.L., Yoon, S.S., 2021. Reusable filters augmented with heating microfibers for antibacterial and antiviral sterilization. ACS Appl. Mater. Interfaces 13, 857–867.

Klemeš, J.J., Fan, Y.V., Tan, R.R., Jiang, P., 2020. Minimising the present and future plastic waste, energy and environmental footprints related to COVID-19. Renew. Sustain. Energy Rev. 127, 109883.

Konda, A., Prakash, A., Moss, G.A., Schmoldt, M., Grant, G.D., Guha, S., 2020. Aerosol filtration efficiency of common fabrics used in respiratory cloth masks. ACS Nano 14, 6339–6347.

Kumar, S., Karmacharya, M., Joshi, S.R., Gulenko, O., Park, J., Kim, G.H., Cho, Y.K., 2020a. Photoactive antiviral face mask with self-sterilization and reusability. Nano Lett. 21, 337–343.

Kumar, A., Sharma, A., Chen, Y., Jones, M.M., Vanyo, S.T., Li, C., Visser, M.B., Mahajan, S.D., Sharma, R.K., Swihart, M.T., 2020b. Copper@ZIF-8 core-shell nanowires for reusable antimicrobial face masks. Adv. Funct. Mater. 31, 2008054.

Kwak, J.I., An, Y.J., 2021a. Microplastic digestion generates fragmented nanoplastics in soils and damages earthworm spermatogenesis and coelomocyte viability. J. Hazard. Mater. 402, 124034.

Kwak, J.I., An, Y.J., 2021b. Post COVID-19 pandemic: biofragmentation and soil ecotoxicological effects of microplastics derived from face masks. J. Hazard. Mater. 416, 126169.

Leung, N.H.L., Chu, D.K.W., Shiu, E.Y.C., Chan, K.H., McDevitt, J.J., Hau, B.J.P., Yen, H. L., Li, Y., Ip, D.K.M., Peiris, J.S.M., Seto, W.H., Leung, G.M., Milton, D.K., Cowling, B. J., 2020. Respiratory virus shedding in exhaled breath and efficacy of face masks. Nat. Med. 26, 676–680.

Li, T., Chen, C., Brozena, A.H., Zhu, J.Y., Xu, L., Driemeier, C., Dai, J., Rojas, O.J., Isogai, A., Wagberg, L., Hu, L., 2021. Developing fibrillated cellulose as a sustainable technological material. Nature 590, 47–56.

Li, Z., Chen, J., Cao, W., Wei, D., Zheng, A., Guan, Y., 2018. Permanent antimicrobial cotton fabrics obtained by surface treatment with modified guanidine. Carbohydr. Polym. 180, 192–199.

Li, S., Donner, E., Xiao, H., Thompson, M., Zhang, Y., Rempel, C., Liu, Q., 2016. Preparation and characterization of soy protein films with a durable water resistance-adjustable and antimicrobial surface. Mater. Sci. Eng. C 69, 947–955.

Lysytsya, A., Mandygra, M., 2014. The antiviral action of polyhexamethylene guanidine derivatives. J. Life Sci. 8, 22–26.

Malvika Kaul, C.M., 2004. Fluorescence-based approach for detecting and characterizing antibiotic-induced conformational changes in ribosomal RNA. J. Am. Chem. Soc. 126, 3447–3453.

Monge, F.A., Jagadesan, P., Bondu, V., Donabedian, P.L., Ista, L., Chi, E.Y., Schanze, K.S., Whitten, D.G., Kell, A.M., 2020. Highly effective inactivation of SARS-CoV-2 by conjugated polymers and oligomers. ACS Appl. Mater. Interfaces 12, 55688–55695.

Morgana, S., Casentini, B., Amalfitano, S., 2021. Uncovering the release of micro/nanoplastics from disposable face masks at times of COVID-19. J. Hazard. Mater. 419, 126507.

Ortega, R., Gonzalez, M., Nozari, A., Canelli, R., 2020. Personal protective equipment and Covid-19. N. Engl. J. Med 382, 105.

Pan, Y., Xiao, H., Cai, P., Colpitts, M., 2016. Cellulose fibers modified with nano-sized antimicrobial polymer latex for pathogen deactivation. Carbohydr. Polym. 135, 94–100.

Pan, Y., Xia, Q., Xiao, H., 2019. Cationic polymers with tailored structures for rendering polysaccharide-based materials antimicrobial: an overview. Polymers 11, 1283.

Pan, Y., Xue, Y., Snow, J., Xiao, H., 2015. Tailor-made antimicrobial/antiviral star polymer via ATRP of cyclodextrin and guanidine-based macromonomer. Macromol. Chem. Phys. 216, 511–518.

Parashar, N., Hait, S., 2021. Plastics in the time of COVID-19 pandemic: protector or polluter? Sci. Total Environ. 759, 144274.

Patricio Silva, A.L., Prata, J.C., Walker, T.R., Duarte, A.C., Ouyang, W., Barcelo, D., Rocha-Santos, T., 2021. Increased plastic pollution due to COVID-19 pandemic: challenges and recommendations. Chem. Eng. J. 405, 126683.

Qin, Y., Li, P., Guo, Z., 2020. Cationic chitosan derivatives as potential antifungals: a review of structural optimization and applications. Carbohydr. Polym. 236, 116002.

Quan, F., Rubino, I., Lee, S., Koch, B., Choi, H., 2017. Universal and reusable virus deactivation system for respiratory protection. Sci. Rep. 7, 39956.

Ranney, M., Griffeth, V., Jha, A., 2020. Critical supply shortages—the need for ventilators and personal protective equipment during the Covid-19 pandemic. N. Engl. J. Med. 382, e41.

Rubino, I., Oh, E., Han, S., Kaleem, S., Hornig, A., Lee, S.H., Kang, H.J., Lee, D.H., Chu, K. B., Kumaran, S., Armstrong, S., Lalani, R., Choudhry, S., Kim, C.I., Quan, F.S., Jeon, B., Choi, H.J., 2020. Salt coatings functionalize inert membranes into high-performing filters against infectious respiratory diseases. Sci. Rep. 10, 13875.

Sachan, D., 2020. COVID-19 pandemic has spurred materials researchers to develop antiviral masks. ACS Cent. Sci. 6, 1469–1472.

Seidi, F., Deng, C., Zhong, Y., Liu, Y., Huang, Y., Li, C., Xiao, H., 2021. Functionalized masks: powerful materials against COVID-19 and future pandemics. Small, 2102453.

Shan, X., Zhang, H., Liu, C., Yu, L., Di, Y., Zhang, X., Dong, L., Gan, Z., 2020. Reusable self-sterilization masks based on electrothermal graphene filters. ACS Appl. Mater. Interfaces 12, 56579–56586.

Sun, S., An, Q., Li, X., Qian, L., He, B., Xiao, H., 2010. Synergistic effects of chitosan-guanidine complexes on enhancing antimicrobial activity and wet-strength of paper. Bioresour. Technol. 101, 5693–5700.

Szczepańska, E., Bielicka-Giełdoń, A., Niska, K., Strankowska, J., Żebrowska, J., Inkielewicz-Stępniak, I., Łubkowska, B., Swebocki, T., Skowron, P., Grobelna, B., 2020. Synthesis of silver nanoparticles in context of their cytotoxicity, antibacterial activities, skin penetration and application in skincare products. Supramol. Chem. 32, 207–221.

Tang, P., Zhang, Z., El-Moghazy, A.Y., Wisuthiphaet, N., Nitin, N., Sun, G., 2020. Daylight-induced antibacterial and antiviral cotton cloth for offensive personal protection. ACS Appl. Mater. Interfaces 12, 49442–49451.

Tcharkhtchi, A., Abbasnezhad, N., Zarbini Seydani, M., Zirak, N., Farzaneh, S., Shirinbayan, M., 2021. An overview of filtration efficiency through the masks: mechanisms of the aerosols penetration. Bioact. Mater. 6, 106–122.

Wang, H., Wei, D., Zheng, A., Xiao, H., 2015. Soil burial biodegradation of antimicrobial biodegradable PBAT films. Polym. Degrad. Stab. 116, 14–22.

Wei, D., Wang, H., Ziaee, Z., Chibante, F., Zheg, A., Xiao, H., 2016. Non-leaching antimicrobial biodegradable PBAT films through a facile and novel approach. Mater. Sci. Eng. C 58, 986–991.

Wibisono, Y., Fadila, C.R., Saiful, S., Bilad, M.R., 2020. Facile approaches of polymeric face masks reuse and reinforcements for micro-aerosol droplets and viruses filtration: a review. Polymers 12, 2516.

Zhang, H., Liu, J., Zhang, X., Huang, C., Zhang, Y., Fu, Y., Jin, X., 2019. Design of three-dimensional gradient nonwoven composites with robust dust holding capacity for air filtration. J. Appl. Polym. Sci. 136, 47827.

Zhang, X.G., Mason, P.W., Dubovi, E.J., Xu, X., Bourne, N., Renshaw, R.W., Block, T.M., Birk, A.V., 2009. Antiviral activity of geneticin against dengue virus. Antivir. Res 83, 21–27.

Zhang, D., Xiao, H., 2013. Dual-functional beeswaxes on enhancing antimicrobial activity and water vapor barrier property of paper. ACS Appl. Mater. Interfaces 5, 3464–3468.

Zhong, Y., Seidi, F., Li, C., Wan, Z., Jin, Y., Song, J., Xiao, H., 2021. Antimicrobial/biocompatible hydrogels dual-reinforced by cellulose as ultrastretchable and rapid self-healing wound dressing. Biomacromolecules 22, 1654–1663.

Zhong, Y., Xiao, H., Seidi, F., Jin, Y., 2020a. Natural polymer-based antimicrobial hydrogels without synthetic antibiotics as wound dressings. Biomacromolecules 21, 2983–3006.

Zhong, H., Zhu, Z., Lin, J., Cheung, C.F., Lu, V.L., Yan, F., Chan, C.Y., Li, G., 2020a. Reusable and recyclable graphene masks with outstanding superhydrophobic and photothermal performances. ACS Nano 14, 6213–6221.

Zhong, H., Zhu, Z., You, P., Lin, J., Cheung, C.F., Lu, V.L., Yan, F., Chan, C.Y., Li, G., 2020b. Plasmonic and superhydrophobic self-decontaminating N95 respirators. ACS Nano 14, 8846–8854.